Experimental evidence of gas-mediated heat transfer in porous solids measured by the flash method

Alexander Lauerer, Artem Lunev

▶ **To cite this version:**

Alexander Lauerer, Artem Lunev. Experimental evidence of gas-mediated heat transfer in porous solids measured by the flash method. 2022. ⟨hal-03524631v4⟩

HAL Id: hal-03524631

https://hal.science/hal-03524631v4

Preprint submitted on 30 Aug 2022

HAL is a multi-disciplinary open access archive for the deposit and dissemination of scientific research documents, whether they are published or not. The documents may come from teaching and research institutions in France or abroad, or from public or private research centers.

L'archive ouverte pluridisciplinaire **HAL**, est destinée au dépôt et à la diffusion de documents scientifiques de niveau recherche, publiés ou non, émanant des établissements d'enseignement et de recherche français ou étrangers, des laboratoires publics ou privés.

HAL Authorization

Experimental evidence of gas-mediated heat transfer in porous solids measured by the flash method

Alexander Lauerer[a], Artem Lunev[a,b,*]

[a]*NETZSCH-Geraetebau GmbH, Wittelsbacherstr. 42, Selb, 95100, Bavaria, Germany*
[b]*School of Physics and Engineering, ITMO University, Kronverksky Prospect 49, St. Petersburg, 197101, Russia*

Abstract

Laser/light flash analysis (LFA) is becoming an increasingly popular assessment tool for the thermal properties of porous samples. Elevated temperature measurements are typically conducted under a protective atmosphere; specifically, under inert gas flow. Immersing a sample with interconnected porosity in a gas environment theoretically allows heat transfer via gas conduction or convection. To prove that LFA measurements are affected by the choice of the gas environment, measurements are conducted under inert gas flow (helium and nitrogen), static inert gas (nitrogen) and vacuum with two different instruments and two sets of samples: highly-conductive alloy foams and insulating lightweight concrete. A heat conduction model accounting for light penetration was used to extract the apparent thermal diffusivity of the solid-gas mixture. A correlation between the Biot number and the conductivity of the gas environment was registered. This is unusual for an LFA experiment where radiative heat losses, which are independent of the gas environment, are typically considered to be dominant. At the same time, variations in either the microgeometry of the porous sample or the type of carrier gas produce a systematic change in the shape of the time-temperature profiles and the duration of the temperature transient. In lightweight concrete samples, switching the instrument to helium flow enables a multifold increase in the apparent thermal diffusivity relative to the measurements done under vacuum. An attempt to explain this variation was made with a two-temperature model of coupled solid-gas conduction. It is argued that an additional factor is missing from the analysis.

Keywords: thermophysical properties, laser flash analysis, porous materials, heat conduction, convection

1. Introduction

Most standard laser-flash and light-flash analysis (LFA) instruments operate under an inert atmosphere. At high temperatures, an inert gas flow suppresses oxidation and minimises the re-deposition of contaminant gases. At ambient and low temperatures, a purge gas ensures smooth temperature manoeuvring by acting as an efficient coolant. The choice of the purge gas species should be informed by: the target temperature range, gas thermal properties and other factors e.g. the gas ionisation potential when electric discharge is highly probable. While the gas environment should

*Corresponding author
Email addresses: alexander.lauerer@netzsch.com (Alexander Lauerer), artem.lunev@metalab.ifmo.ru (Artem Lunev)

always be compatible with a safe operation of the instrument, it might also affect the time-temperature transients intrinsic to the material under study. Ultimately, this is reflected in biased measurement results. Such bias might arise when measuring open-cell foams [1] or powder compacts [2]. There, the purge gas is able to freely roam the pore space. Because a potential contribution from the purge gas is expected, the reported values of thermal properties risk turning into *ad hoc* "effective" quantities with an undefined range of validity. With regards to LFA measurements of porous materials, some researchers [3] had preferred low-conductivity purge gases such as nitrogen. Others had used a more conductive helium [4, 5, 6, 7, 8]. Attempts to explain the variation of thermal diffusivity with the gas environments do exist [9]. At the same time, these explanations relate only to the scaling of the time axis in the LFA experiments due to the definition of the Fourier number as $\mathrm{Fo} = at/l^2$, where a is the thermal diffusivity, t is the time and l is the path of thermal diffusion. It is unknown whether linear scaling is only expected or if nonlinear processes are at play e.g. resulting in a change of concavity of the heating curves. This issue seems overlooked although the thermal properties of porous materials are in focus of many ongoing research activities. There has been a growing interest in applying the LFA technique to measure metal and ceramic foams [10, 11, 12], coal [13], zeolites [14], concrete [15, 16] and other promising materials.

In contrast to other measurement techniques such as the transient plane source (TPS) method [17] or the guarded hot plate method (GHP) [18], flash measurements produce shorter temperature transients of a small magnitude resulting in fairly low temperature gradients. Under these conditions, the dynamic gas flow caused by natural convection is normally considered negligible, viz. Section 2.3 in [9]. When analysing the "raw" time-temperature profiles measured experimentally, the contribution of gas conduction inside the porous matrix is typically ignored completely. Indeed, models of heat conduction in a rod (Cowan [19] – as used in [9]) or a solid cylinder (Cape-Lehman [20]) are employed. After evaluation, a variation in thermal conductivity λ of porous materials is typically registered under different gas environments. This variation is explained in terms of effective-medium models also known as mean-field or self-consistent methods, SCMs. An example is the Bruggeman model referenced in [9]. The theoretical framework giving rise to SCMs is sometimes referred to as the Maxwell's approach with a notable result being the Maxwell-Garnett relation. Limitations of the Maxwell's approach had previously been discussed in [21] for non-overlapping, non-interacting inclusions. Limitations of empirical SCMs including the Bruggeman model have recently been assessed in [22]. In short, an SCM may provide means to reduce a heterogeneous structure formed of many inclusions (λ_i) in a matrix (λ_m) to a single particle with "effective" properties. The homogenisation procedure used to arrive at this result considers steady-state heat diffusion described by the Laplace's equation: $\Delta T = 0$, where Δ is the Laplace operator and T is the temperature. Since a transient heat equation includes a time derivative $\partial T/\partial t$, the homogenisation procedure formulated under static conditions is not guaranteed to work in the dynamic mode. As a result, the "effective" transport properties for the steady-state and transient heat transfer would likely be different. Evidence of the latter has been recently presented in [1].

Unfortunately, papers reporting on LFA measurements in porous materials seldom provide sufficient details of how raw data (voltage over time) is converted into the reported thermal diffusivity values, a. As a consequence, it

is impossible to estimate the error inherent to this procedure. This was in focus of a recent research [23, 24, 25] where a typical deviation of the heating curve had been demonstrated in porous rocks. Sophisticated models based e.g. on the Guyer-Krumhansl equations or the two-temperature ($2T$) approach had been employed to mitigate this problem. The authors findings [23, 24, 25] have additionally been confirmed in a recent paper on metal foams [1] providing further insights into the non-Fourier behaviour of porous materials under temperature transients. One of the key results [1] indicates the porosity distribution alters the curvature of the heating curve registered experimentally. One of the causes for this deviation is the three-dimensionality of heat fluxes in a porous system. It is unknown though whether changing the gas medium could also distort the shape of the heating curve.

This work aims to close this gap. It explores how a gas environment might affect the heat transfer pathways activated in a LFA measurement of highly-conductive and insulating porous materials. Secondly, the feasibility of using the LFA to measure the thermal properties of a porous material in a gas environment is investigated.

2. Experimental

2.1. LFA Measurements

The physical phenomenon of interest is demonstrated using two commercial, mainstream instruments. The LFA 457 [26] (near-IR laser source) and LFA 467 (xenon lamp) instruments are used, with differing geometries of the gas and cooling channels, the direction of the gas flow (top-to-bottom in LFA 467 and bottom-to-top in LFA 457), and vacuum capabilities. Measurements could be conducted either under a defined inert gas flow with a default value of 100 ml/min, under vacuum or in a static atmosphere. The LFA 457 could be continuously evacuated using an external rotary pump during the whole measurement duration. The instrument was configured to deliver 0.35 ms laser pulses at a lamp voltage of 1538 V. The LFA 467 produced 0.6 ms xenon pulses (250 V), which resulted in a somewhat lower sample heating compared to the laser instrument. In both instruments, pulse shapes were recorded at each flash and stored for subsequent pulse correction.

For each material tested (see Section 2.2), three series of measurements were carried out in a pre-specified temperature range — first, when purging the instrument chamber with helium, then with nitrogen, then under dynamic vacuum. Additionally, measurements under a static inert atmosphere were conducted in the thermally-insulating material. When comparing purge gases, it should be noted that the thermal conductivity of helium ($\lambda_g = 0.15$ W/m·K) was significantly higher than in nitrogen ($\lambda_g = 0.025$ W/m·K).

All porous samples were measured without any graphite coating. Uncoated surfaces tend to have lower emissivity, decreasing the amount of radiative heat losses. This reduces the uncertainty due to the possible radiative heat transfer contribution. Contrary to the experimental conditions in [9, 27], a lack of surface coating allows the light to penetrate through the bulk of the samples with open porosity. Light penetration is a source of uncertainty – but it can be eliminated completely using an appropriate modification of the evaluation procedure while measuring sufficiently thick samples. This is different from the approach taken in [9, 27] where the samples are rendered opaque by filling

the outermost pores with a thin paste layer. Obviously, this eliminates light penetration. However, as explained previously in [1], the paste layer participates in the heat transfer. Since the paste and the material under study are dissimilar, heat fluxes across their interfaces must overcome a thermal contact resistance. The presence of a third phase (the paste) in additional to the other two (the matrix material and the porosity) is highly undesirable if accurate measurements need to be conducted. It is nearly impossible to account for that additional source of uncertainty. At the same time, uncoated porous samples are not opaque, making flash-throughs possible. To avoid flash-throughs during the laser/light shots and reduce stray light, the samples needed to be sufficiently thick. This helps to eliminate a distortion of the measurement results similar to the one reported in [28].

2.2. Materials

Experimental samples included two sets:

- Aluminium-magnesium foams fabricated by Exxentis AG (Wettingen, Switzerland), with 60% (open) porosity and a density of 1.09 g/cm^3. Samples with a nominal pore size of 0.20 – 0.35 mm and 0.40 – 1.00 mm were tested. The matrix material is very conductive – hence fast transients are expected;
- Lightweight concrete samples fabricated by Ytong, with densities $\rho_m = 0.52$ g/cm^3 and 0.54 g/cm^3. Contrary to the previous material, Ytong is thermally insulating, producing long transients.

Samples from both available materials were prepared in a cylindrical geometry, with a thickness of 5 mm and a diameter of 12.5 mm. The samples under study had open porosity permeable to the surrounding gas. Al-Mg foams were measured exclusively with LFA 457, whereas Ytong was measured both with LFA 457 (static atmosphere and vacuum) and LFA 467 (gas flow).

2.3. Data processing

After collecting the time-temperature profiles $T(t)$, the latter were exported in a `csv` format and loaded into PULsE [29] (version 1.93F [30]), an open-source numerical analysis software, to extract the thermal diffusivity values from the raw data.

2.4. Model accounting for light penetration

The data was processed with a "Penetration model", which accounted for a spatially distributed absorption of the laser pulse at the sample front and distributed emission of the thermal radiation measured by the detector at the rear of the sample. The original problem statement can be found, e.g., in [31] or [32]. In both cases, it is limited to a infinitesimal pulse generating an initial nonuniform temperature profile. PULsE allows an additional finite-pulse correction based on the experimental pulse diode data.

The boundary problem considered in PULsE is:

$$\frac{\partial \theta}{\partial \mathrm{Fo}} = \frac{\partial^2 \theta}{\partial y^2} + \Phi(\mathrm{Fo})\Psi(y), \tag{1a}$$

$$\left.\frac{\partial \theta}{\partial y}\right|_{y=0} = \mathrm{Bi}\cdot\theta\Big|_{y=0}, \tag{1b}$$

$$\left.\frac{\partial \theta}{\partial (-y)}\right|_{y=1} = \mathrm{Bi}\cdot\theta\Big|_{y=1}, \tag{1c}$$

$$\theta(y,0) = 0, \tag{1d}$$

written for dimensionless heating θ, time Fo and axial coordinate y (for the definition of these variables, the reader is referred to [33]). In this formulation, both radiative and gas-driven heat losses are linear and sum up to the Biot number, Bi. The volumetric energy density $\Psi(y)$ absorbed by the sample may be derived from the Beer-Lambert law and the continuity equation, yielding $\Psi(y) \propto \gamma \exp(-\gamma y)$, where the parameter γ is the laser absorptivity divided by the sample thickness, l. Because temperature is measured in arbitrary units, the proportionality factor may be omitted. $\Phi(\mathrm{Fo})$ refers to a normalised pulse temporal shape. Following [31], the detector registers the sum of contributions from a range of $\theta(y)$ values: $V \propto \int_0^1 \theta(y)\exp(-\gamma_1 y)\mathrm{d}y$, where γ_1 is the absorptivity of thermal radiation.

Equation (1) is solved with a fully-implicit finite-difference solver based on the Thomas algorithm [33]. For a given time step τ and a grid spacing h this is $O(h^2+\tau)$ accurate. The solution has been benchmarked against Proteus LFA Analysis where an analytical solution is implemented based on [32]. At $\gamma_1^{-1} = 0$ and an infinitesimal pulse, both models gave identical results when processing data from standard test samples. In the following calculations, it is assumed that the absorption of the incoming (laser/light) and induced (thermal) radiation are equal: $\gamma = \gamma_1$. Example $\theta(\mathrm{Fo})$ solutions of Equation (1) are shown in Figure 1 at $\gamma = 10$ and $\gamma = \infty$. An infinite value of γ corresponds to a heat source localised at $y = 0$, which reduces to the standard model. The standard and the adiabatic models are described in the Supplementary Material, Section S.1.

Another important point is the optimisation procedure needed to reverse-engineer the material thermal properties from the measured time-temperature profiles. To avoid the influence of data outliers sometimes observed in the time-temperature profile, the sum of absolute deviations, rather than sum of squared residuals, was used as an objective function metric f:

$$f = \frac{1}{n_e - n_s}\sum_{i=n_s}^{n_e}\left|V(\widetilde{t_i}) - \widehat{\theta}(\widetilde{t_i})\right|, \tag{2}$$

where $V(\widetilde{t_i})$ is a detector voltage value proportional to the rear-face heating measured at time $\widetilde{t_i}$; $\widehat{\theta}(\widetilde{t_i})$ is the scaled solution of Equation (1) interpolated specifically at time $\widetilde{t_i}$ using natural cubic splines; n_s and n_e are the end points of the search domain. Since the standard Levenberg-Marquardt algorithm only allows a least-squares objective function, a BFGS/Wolfe nonlinear optimiser described in [33] was employed to handle f. A comparison of optimisation using ordinary least-squares and absolute deviations is provided in the Supplementary Material, Section S.2.

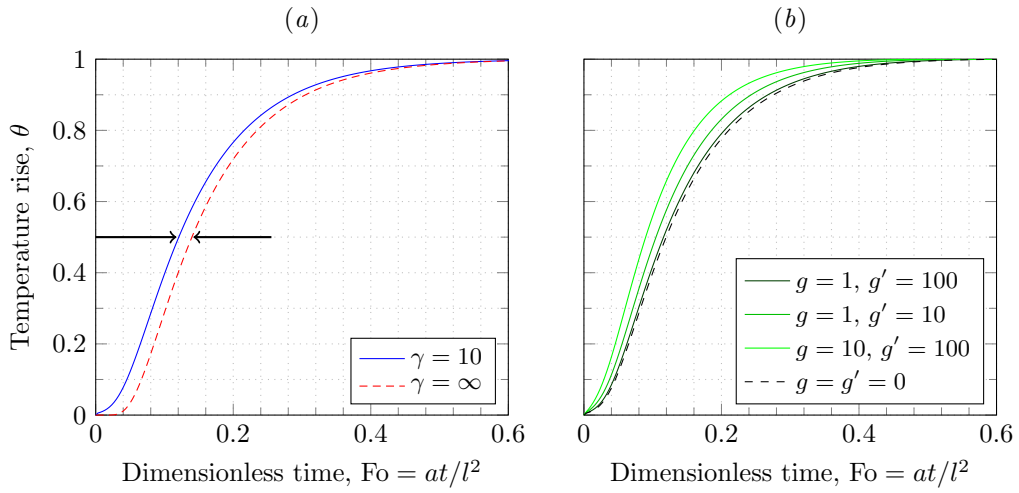

Figure 1: Dimensionless temperature rise curves $\theta(\mathrm{Fo})$ (*a*) for the model (1) calculated at $\gamma = 10$ and $\gamma = \infty$, showing the accelerated temperature response at a finite γ; (*b*) for the $2T$ model at $\gamma = 10$ in helium at various g, g' combinations.

At each test temperature, the thermal diffusivity value was averaged typically over five shots. The statistical error was calculated assuming a 95% confidence level. Details on these calculations are provided in the Supplementary Material, Section S.4.

2.5. Two-temperature (2T) model

The experimental conditions described in Section 2.1 imply that heat is non-uniformly absorbed in the porous body. The solid phase absorbs most of the incoming flash energy. Consequently, it responds to the heating faster than the gas phase. This produces a temperature difference $(T^{(s)} - T^{(g)})$ between the solid and the gas phase. When energy exchange g between these two systems is negligible, the problem statement (1) holds. When this condition is not met, an additional coupling term $G(T^{(g)} - T^{(s)})$ needs to be introduced into the heat equation, viz. [34]. The two-temperature model in porous solids has been used previously e.g. in [23, 35].

It is convenient to introduce short-hand notations: $u_t = \partial u/\partial t$ and $u_{tt} = \partial^2 u/\partial t^2$. The heat equation in (1) is modified by introducing the coupling term:

$$\theta^{(s)}_{\mathrm{Fo}} = \theta^{(s)}_{yy} + \Phi(\mathrm{Fo})\Psi(y) + g(\theta^{(g)} - \theta^{(s)}), \tag{3}$$

where $g = Gl^2/[(1-\varepsilon)\lambda^{(s)}]$ and the porosity ε is introduced.

Assuming no contribution from convection, the gas conduction follows the equation:

$$\theta^{(g)}_{\mathrm{Fo}} = \left(\frac{a_g}{a_s}\right)\theta^{(s)}_{yy} + g\left(\frac{1-\varepsilon}{\varepsilon}\frac{C_p^{(s)}\rho^{(s)}}{C_p^{(g)}\rho^{(g)}}\right)(\theta^{(s)} - \theta^{(g)}), \tag{4}$$

where the quantities a_i, C_p^i and ρ^i indicate the thermal diffusivity, specific heat and density of the phase $i = (g), (s)$. The Fourier number in both Equation (3) and Equation (4) is defined as $\mathrm{Fo} = a_s t/l^2$. The temperature scaling factor is the same for both $\theta^{(s)}$ and $\theta^{(g)}$: $\theta^i = (T^i - T_0^i)/\delta T_{\mathrm{Inf}}$ at $i = (g), (s)$.

Note the dimensionless equations (3) – (4) are very similar to the ones considered in [35]. Without going into details of the pore arrangement, the model is solved numerically, assuming both phases (a) are uniformly distributed across the y axis and (b) exchange heat with the static surroundings at their $y = 0$ and $y = 1$ external boundaries. This gives rise to the boundary conditions of cooling viz. Equation (1). The finite-difference scheme for this model is given in the Supplementary Material, Section S.6.

The model given by Equations (3) and (4) introduces two additional unknown parameters: the dimensionless coupling coefficient g and the gas Biot number $\mathrm{Bi_g}$. These parameters are determined from optimisation. Gas thermal properties are assumed known. Indeed, the specific heat $C_p^{(g)}$ may easily be calculated using the equation-of-state. At the same time, $\rho^{(g)}$ is more difficult to define. It depends on the pressure inside the pores, which may roughly be deduced from the Laplace equation. It is not practical to try calculating this pressure with just the laser flash experimental data. Instead, the coupling factor $g' = (1-\varepsilon)/\varepsilon[C_p^{(s)}\rho^{(s)}]/[C_p^{(g)}\rho^{(g)}]$ in (4) may be regarded as an unknown parameter. Typically [35], $g = 0.1 - 20$ and $g' > g$. An example calculation of $\theta^{(s)}(\mathrm{Fo})$ with the $2T$ model is shown in Figure 1 (b). Compared to model (1), the $2T$ model shows a similar shift of the half-time $t_{1/2}$. The onset of heating seems to be less affected by the coupling term. Largest differences appear at the late heating stages. Here, the temperature equilibration seems to lag behind the prediction of the unperturbed $g = g' = 0$ solution. Interestingly, Equations (3) and (4) may be combined, resulting in the so-called dual-phase lag (DPL) model [36]. There are other variants of the DPL model including the Jeffreys type equation, criticised in [37, 38].

3. Results

3.1. Al-Mg foams

Thermal diffusivity measurements of metal foams are conducted under two purge gas species and under dynamic vacuum at temperatures $T = 25$ – 450 °C. The variation of thermal parameters in metal foams with pore size at constant porosity has recently been assessed in LFA experiments in [1]. At the same time, the impact of gas-mediated heat transfer was not initially clear. Its influence on the diffusivity values is shown in Figure 2.

Thermal diffusivity was calculated with the model (1) based on the experimental time-temperature profiles in two cases: (a) when γ was allowed to vary and (b) using γ values extracted from the computed tomography (CT) data in [1]. A ray-casting algorithm was employed in [1] to evaluate the cross-sectional mean of the projected area distribution function from CT scans. The axial dependence of the latter was used to fit $A\exp(-\gamma y)$ as a function of the dimensionless coordinate y. The "real" γ value characterising light attenuation and the γ value calculated as a parameter to the heat conduction problem differ. Logically, this manifests in different a values determined using both approaches. Table 1 shows an uncertainty in the γ determination may lead to qualitatively different conclusions on

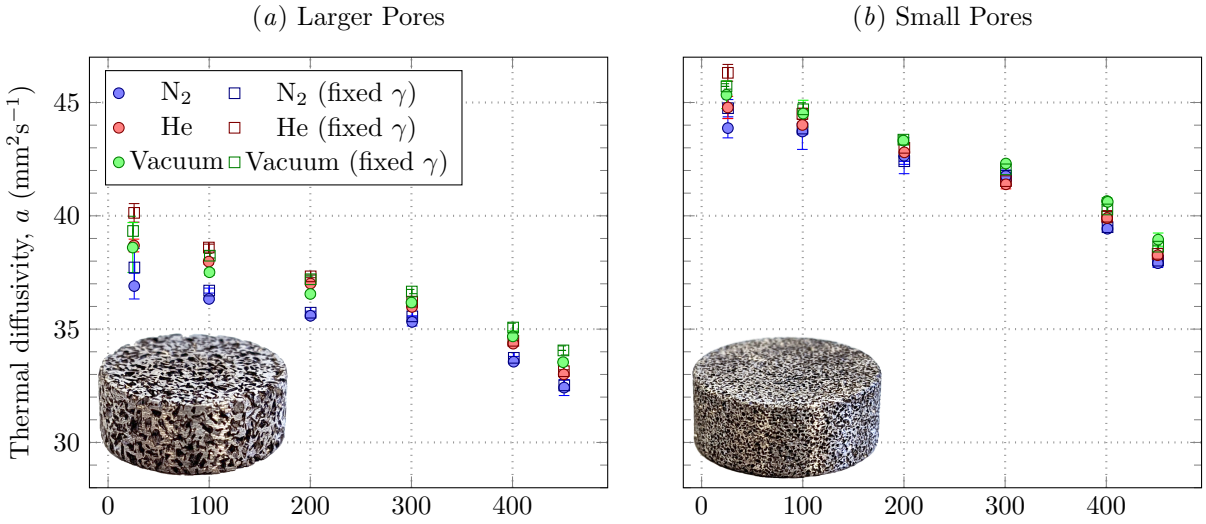

Figure 2: Apparent thermal diffusivity of Al-Mg foams measured in various gas environments. Two cases are considered: γ as an optimisation parameter; and a fixed γ corresponding to the rigorous CT-FEA modelling in [1]. Note that the "thermal diffusivity" measured under vacuum is slightly higher compared to both measurements under a gas environment. This indicates the simple analysis is inapplicable in case of metal foams.

the influence of gas. For instance, thermal diffusivity calculated in small-pored samples measured under helium may either be lower or higher compared to vacuum measurements, depending on which way the γ value was derived. Still, the measurements done under vacuum result in a higher thermal diffusivity value compared to nitrogen. This variation cannot be explained consistently using the available effective-medium models, such as those used in [9]. The likely reason for this discrepancy are the non-Fourier effects previously reported in [1].

For convenience, the thermal parameters extracted from room-temperature measurements of metal foam samples under varying gas environment and microgeometry are summarised in Table 1. Additionally, Figure 3 shows example room-temperature data and model solutions for samples with small pores. The span of the temperature transient may be characterised by the time $t_{1/2}$ required for the rear surface to reach half of the maximum temperature rise [39]. This quantity is affected by the heat losses [40]. The difference between using an adiabatic two-parameter pulse-corrected model and the model (1) seems small when analysing the datasets displayed in Figure 3 (*b*) and (*c*). The Biot number is small under nitrogen and near-zero under vacuum, thanks to the high conductivity of the sample and short measurement times. The half-time values may also be affected by the solid-gas thermal coupling, as seen from Figure 1 (*b*). This likely adds to the overdiffusive temperature behaviour in metal foams already observed under vacuum.

The solutions obtained with the model (1) were in close agreement with the experimental datasets displayed in Figure 3. Simpler models with fewer parameters including the adiabatic model and the standard model were also considered (a detailed description may be found in the Supplementary Material, Section S.1). Unfortunately, these models were judged unsuitable for data processing, especially in samples with large pores, based on a statistical

Table 1: Mean values of thermal properties calculated by averaging over a series of five measurements in metal foams with large and small pores at room temperature under different gas environments. The full version of this table may be found in the Supplementary Materials, Table S2.

Parameter		Large pores (0.40 - 1.00 mm)			Small pores (0.20 - 0.35 mm)		
		He	N_2	Vacuum	He	N_2	Vacuum
$t_{1/2}$ (s)		0.077 ± 0.002	0.086 ± 0.001	0.084 ± 0.004	0.072 ± 0.001	0.0765 ± 0.002	0.0749 ± 0.0008
a (mm^2 s^{-1})	[1]	$\mathbf{38.69 \pm 0.28}$	36.90 ± 0.60	38.30 ± 0.90	44.72 ± 0.33	43.90 ± 0.40	$\mathbf{45.30 \pm 0.60}$
	[2]	$\mathbf{40.13 \pm 0.41}$	37.72 ± 0.84	39.33 ± 0.65	$\mathbf{46.31 \pm 0.37}$	44.75 ± 0.38	45.71 ± 0.12
γ	[1]	13.18 ± 0.36	13.60 ± 1.10	13.90 ± 1.30	25 ± 2	23 ± 4	30 ± 20
	[2]	16.45			39.8		
Bi	[1]	0.074 ± 0.008	0.025 ± 0.005	0.007 ± 0.008	0.084 ± 0.007	0.013 ± 0.009	0.003 ± 0.004

[1] γ as an optimisation parameter

[2] γ derived from the absorption profile in [1]

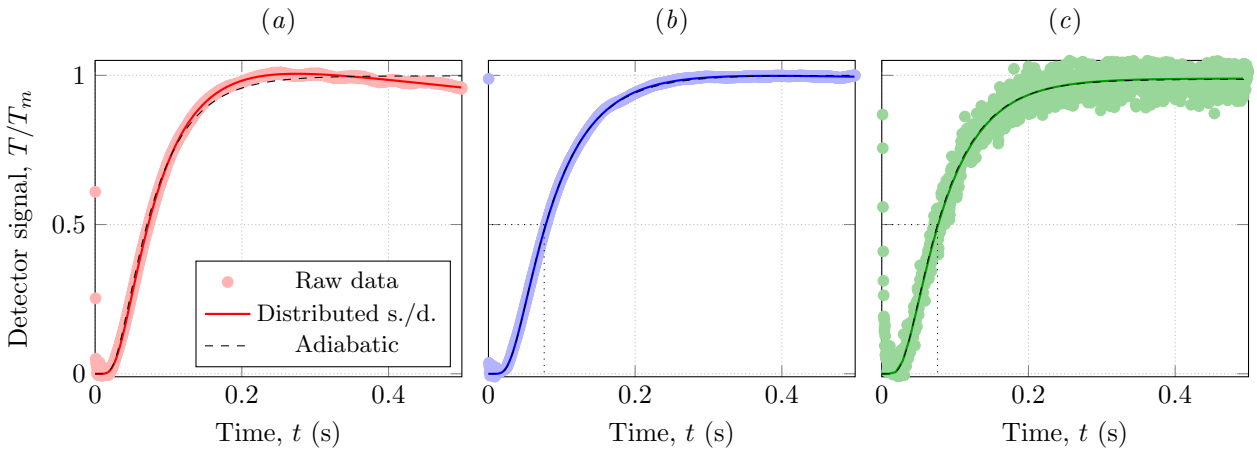

Figure 3: Baseline-subtracted time-temperature profiles showing raw data (markers) and model solutions (solid lines) at room temperature in Al-Mg foams (small pores). Measurements done under (*a*) helium, (*b*) nitrogen and (*c*) vacuum. Curves calculated with the classical adiabatic, pulse-corrected model ($\gamma^{-1} \equiv 0$, Bi $\equiv 0$) are shown in black dashed lines.

comparison. Details on model selection are presented in the Supplementary Material, Table S1 and in Section S.3. Overall, the model (1) seemed to produce a much better fit. The reason for this was, again, the additional parameter, γ. The latter is usually optimised simultaneously with a, Bi and T_{Inf}. When this approach was taken, a small variation in γ could be registered, see Table 1. This variation was difficult to detect in case of metal foams due to its low magnitude. The variation in the "effective" γ depending on the gas species was also lower compared to the difference between the "true" γ values determined from the light absorption profile and the average "effective" γ. This difference likely comes from the influence of the microgeometry [1]. At the same time, the small variations in the "effective" γ are correlated with the gas carrier. In metal foams, a lower γ value seems to be characteristic of a more conductive carrier gas, in this case, helium.

The signal-to-noise data is seen to decrease under vacuum, see Figure 3 (c), when there is no coolant gas necessary for efficient temperature manoeuvring at or slightly above ambient temperature. Therefore, small random temperature fluctuations appear. At the same time, the laser heating in a sample without a high-emissivity coating is also small. Therefore, the raw data displays high noise. This noise does not pose any problems to the optimisation procedure. The latter was shown to be stable to both Gaussian and Laplacian noise of various magnitudes (see Supplementary Material, Section S.5). Finally, it should be noted that, under helium, a direct contribution from either convection or gas conduction results in a pronounced cooling segment, see Figure 3 (a).

Summing up the above, in metal foam samples, a change in the gas carrier species in LFA measurements promotes a lagging temperature response. This affects the thermal diffusivity value, a. Variations in the thermal diffusivity of metal foams under different gases cannot be consistently explained with the effective-medium models considered earlier.

3.2. Ytong

Lightweight concrete samples were measured under a gas flow (nitrogen and helium), under vacuum and under a static nitrogen atmosphere at test temperatures $T = 25$ – 120 °C. Such measurements require very long acquisition times due to low thermal diffusivity values and a thick sample. To ensure accurate results, temperature should be very stable over an extended period of time. This is difficult to achieve under a static nitrogen atmosphere or under vacuum (both measurements done in LFA 457, as opposed to measurements under a gas flow done in LFA 467). In most cases, a strong linear drift in the baseline detector signal could easily be corrected for. However, when measurements required particularly long acquisition times, random deviations from this trend were observed. Obviously, the purge gas also acts as a coolant for the heater and ensures smooth temperature manoeuvring at low temperatures when radiation cooling is ineffective. When the chamber pressure drops or when no gas flow is maintained, temperature equilibration is made more difficult. This explains the error margin in measurements under vacuum or under a static atmosphere shown in Figure 4. As Ytong samples crumble if an excessive load is applied, extra care was taken to preserve the integrity of the samples.

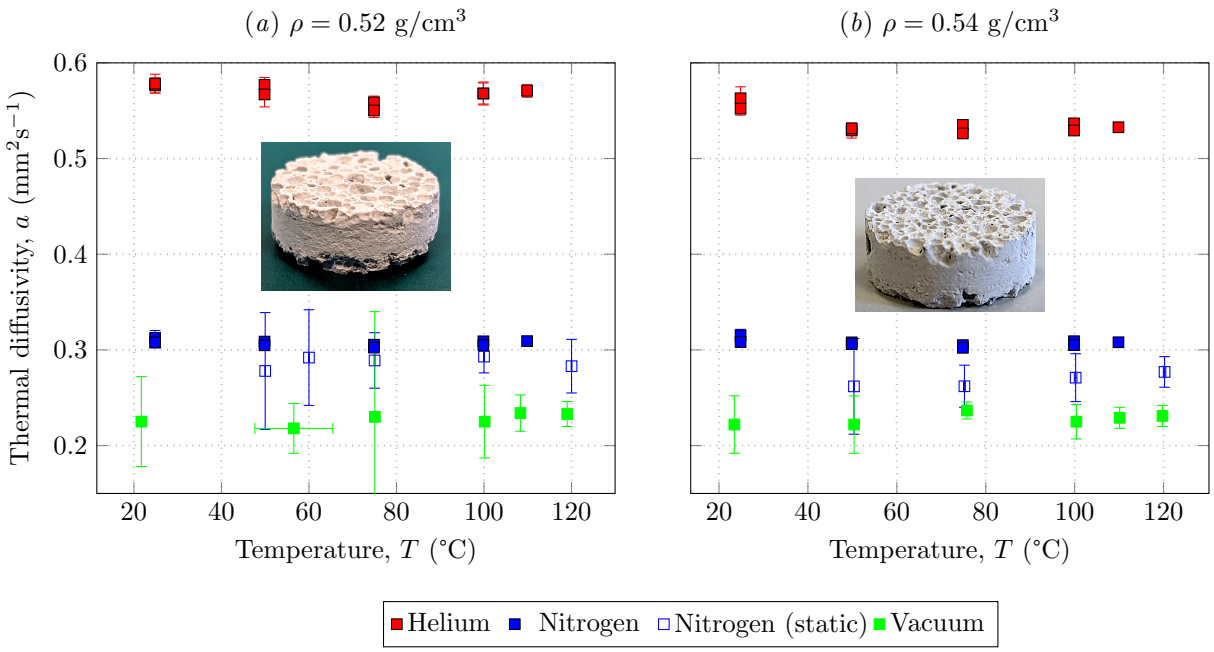

Figure 4: Apparent thermal diffusivity of Ytong lightweight concrete samples measured under various gas environments. At each test temperature for the datasets corresponding to helium and nitrogen flow, two markers are plotted indicative to the measurements done respectively during the heating and cooling stages.

The measurement results indicate that any change in atmosphere severely affects the magnitude of thermal diffusivity in Ytong. In helium, Ytong appears more conductive whereas nitrogen results in temperature transients twice as long (Figure 5). At the same time, the apparent thermal diffusivity of Ytong samples under both gases is significantly higher than under vacuum.

The values of the model parameter γ estimated under various gas environments show a peculiar trend. The calculated γ values in Ytong are strongly dependent on the gas species (Table 2). Unlike metal foams, Ytong displays a larger γ value in helium and the lowest γ value under vacuum. This is reproducible in both samples. Lower γ values indicate a sharper initial onset of the curves, which is observed in Figure 5. It is unlikely that any of the gases could significantly affect light penetration within the sample volume. An attempt was made to explain this discrepancy using the two-temperature model. To allow realistic estimates, these parameter values were fixed: $\gamma = 9.8$ and $a = 0.23$ mm$^2 s^{-1}$. Additionally, g and g' were optimised. The results of this calculation are shown in Figure 6. A fair agreement between the raw data and the model solution was observed under nitrogen. This likely indicates the variation in the effective thermal diffusivity observed in Figure 4 might be explained by the coupled conduction in the solid and the gas phase. In case of helium, the solution appears significantly different from the trends displayed by the raw data. This has led us to believe that the $2T$ model might either be not fully applicable or an unknown contribution appears.

As opposed to the considerably higher conductive metal foams, Ytong displays significant heat losses, see Figure 5 and Table 2. The Biot number, which should be representative of either radiative or gas-mediated cooling, is very high

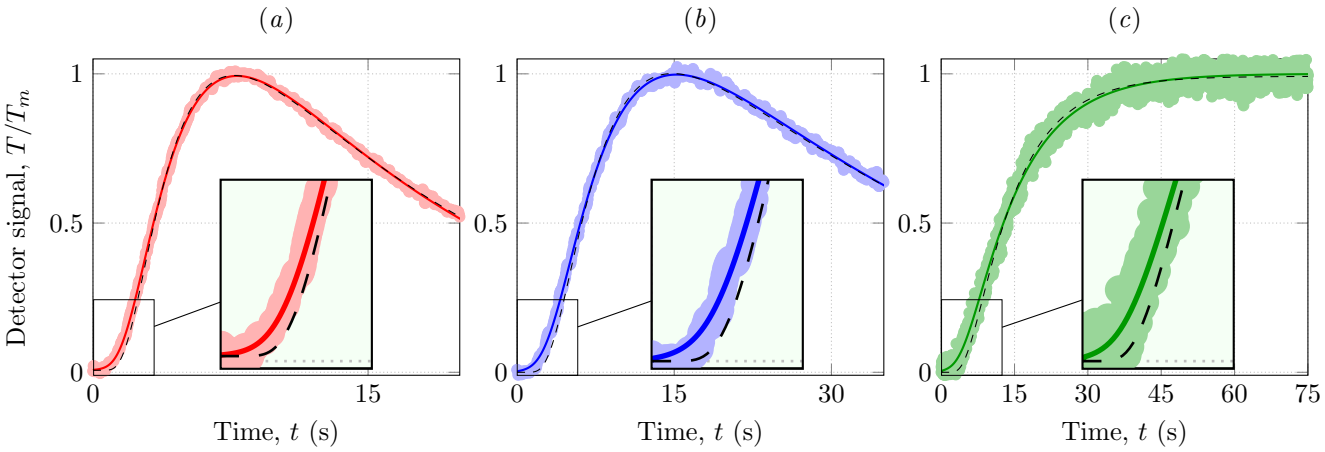

Figure 5: Baseline-subtracted time-temperature profiles showing raw data (markers) and model solutions (solid lines) at room temperature in Ytong ($\rho = 0.54$ g/cm^3). Data is shown from measurements done under (*a*) helium, (*b*) nitrogen and (*c*) vacuum. The model solutions correspond to the following Biot values in Equation (1): (*a*) 2.12, (*b*) 1.68 and (*b*) $\simeq 0$. To illustrate the difference between Equation (1) and a model where the heat source is localised at front surface, results of a constrained calculation with a zero distributed heat source ($\gamma^{-1} \equiv 0$) are shown in black dashed lines.

Table 2: Mean values of thermal properties calculated by averaging over a series of five measurements in Ytong ($\rho = 0.52$ g/cm^3) at $T_0 =$ 21-50 °C under various gas environments. The full version of this table may be found in the Supplementary Materials, Table S3.

Parameter	Gas environment			
	He	N_2 (dynamic)	N_2 (static)	Vacuum
T_0 (°C)	24.85	24.85	50.0 ± 0.1	21.2 ± 0.7
a (mm^2 s^{-1})	0.576 ± 0.008	0.312 ± 0.008	0.28 ± 0.06	0.23 ± 0.05
γ	11.27 ± 0.22	10.4 ± 0.3	9.8 ± 1.2	9.7 ± 4.8
Bi	2.17 ± 0.07	1.63 ± 0.11	1.23 ± 0.8	0

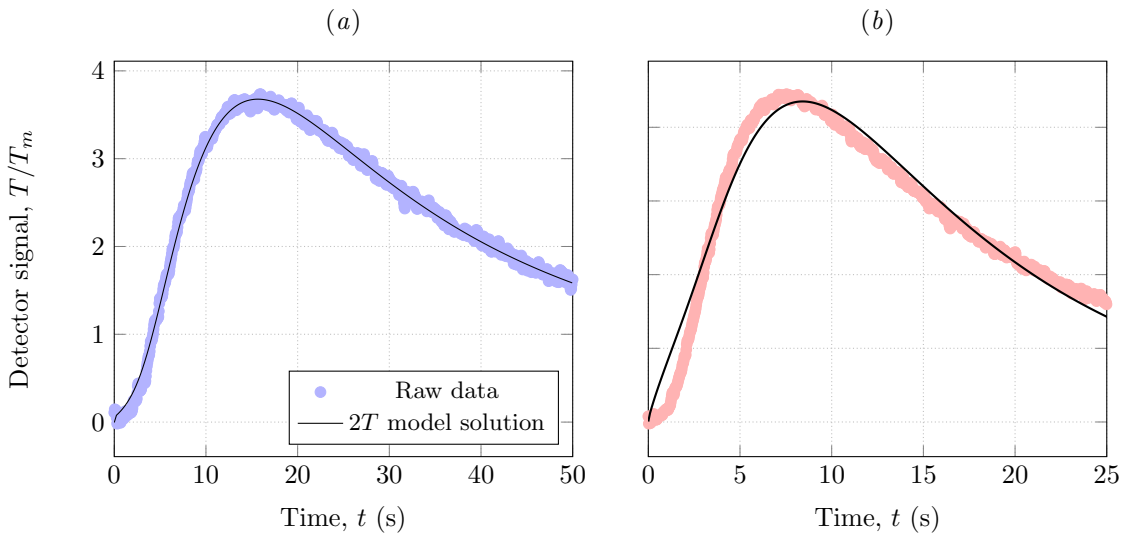

Figure 6: Raw data and optimised solutions with the two-temperature model (3) – (4) corresponding to measurements under (*a*) nitrogen ($g = 1.22$ and $g' = 0.9657$) and (*b*) helium ($g = 19.74$ and $g' = 1 \times 10^4$).

at room temperatures under a gas flow, reaching values of up to 2.12. At the same time, it is much lower – almost zero – under vacuum. This means that the cooling segment in Figure 5 (*a*) and (*b*) is exclusively associated with the gas environment. Since the temperature maximum is reached after about 90 s as compared to about 15 s in helium, heat transfer in the gas phase within this sample volume may actually be more efficient than conduction.

Another important point is that the time-temperature profiles in all cases could still be described by Equation (1) quite well, showing no significant abnormality in the residual distribution. However, despite the fit being good, this does not mean that the model is correct. One of the key factors producing shorter temperature transients in a Ytong sample placed in a gas environment seems to be the coupling between solid-state thermal conduction, convection and gas-phase conduction.

4. Discussion

The observations made in this work fall in two categories:

(a) Relating to the apparent thermal diffusivity of porous solids depending on the gas species. The increase is more pronounced in lighter, more conductive gases;

(b) Relating to a deviation from the expected behaviour of the heating curve modelled using eq. (1), when γ is representative of light absorption.

The term “apparent” thermal diffusivity is used to highlight that the parameter, a, responds to the way measurements are conducted. Not always a is representative of the material under study (even in the sense of an effective medium).

First, consider the thermal diffusivity of metal foams. Note that diffusivity will change if the sample surface is made opaque. The range of diffusivity values reported in [1] for the small-pored samples under nitrogen is 36-42 $\mathrm{mm^2 s^{-1}}$. Lower values are obtained when the heat propagation path, l, is taken equal to the sample thickness. A longer thermal diffusion path in porous solids is characterised by their tortuosity. On the other hand, there is an advantage of measuring samples with open porosity located at the external surface. Namely, model calculations using Equation (1) do not need to explicity account for the difference between the geodesic and the Euclidean paths. This is explained in more detail in [1]. However, when the samples are made opaque, accounting for tortuosity requires using l equal to the geodesic distance. If l is taken as the Euclidean distance, lower thermal diffusivity values are obtained. When conducting measurements in samples with open porosity, the value of the thermal diffusivity is influenced by γ, the mean absorption depth in the Beer-Lambert law. It may be argued that γ may only be accurately determined when the real absorption profile is know. Therefore, measurements with sealed surface pores (e.g. in [9] and in the second part of [1]) and open surface porosity reported in this work require additional information. This information may be extracted from computed tomography (CT).

At the same time, even knowing the precise light absorption depth or the tortuosity of the material, determining the thermal diffusivity, a, remains challenging. There are fundamental reasons behind this difficulty. Porous samples require adjustments to the macroscopic Fourier law, as explained in [1]. Another reason is the coupling between solid conduction with either gas conduction, gas convection, or both. The two-temperature model [Equations (3) and (4)] offers a way to explain the difference in the apparent thermal diffusivity caused by the gas species by coupling the heat equation of the solid phase with the respective equation for the gas phase. Note that the same model is expected to hold in phase-change materials during the formation of the mushy regions, where a solid and a liquid phase co-exist. At the same time, the deviation of the model solution shown in Figure 6 from the raw data suggests there is a missing factor in the explanation. This points to the possible role of convection. Alternatively, this might be due to purely geometric reasons [35].

Given the above, it is possible that accounting for convection may be necessary to correctly describe the temperature transients in the laser flash experiments. Convection normally gives rise to an additional term in Equation (4), called the advective term [35]. Additionally, convection is usually characterised by the Rayleigh-Darcy number $\mathrm{Ra} = gk\Delta TL/(\nu a_g T_0)$, where g is the gravitational acceleration and k is the permeability of the matrix. Unfortunately, the latter cannot be quantified from the experimental time-temperature profiles directly. Another parameter, the Biot number $\mathrm{Bi} = h\lambda/L$, is directly inferred from the measurements. It can be thought of as the ratio between the resistance to conduction λ/L and resistance to convection h^{-1}. In the previous section, Bi was calculated assuming the gas simply drives away heat from the sample surface to the external volume.

Convection is expected to influence measurement results due to the geometric arrangement of the laser source relative to the sample. In a conventional LFA setup, the sample is arranged vertically, and its bottom part is heated up by the flash. A porous sample in a gas environment is effectively a composite material made of the solid matrix and the gas inside the pores. Following the flash, an energy exchange between the solid and the gas leads to a temperature

increase in the lower parts of the gas sub-system. Colder, and therefore denser, gas portions experience a stronger gravitational pull than the rarefied hot gas as the bottom. This creates conditions for a convective flow. The convective contribution to heat transfer may be estimated based on the formalism provided by Soboleva [41]. In case of one-dimensional heat transfer, the following governing equation of heat transfer applies (here the time derivative of mean pressure dP/dt is assumed zero):

$$[(1-\phi)\rho_m C_m + \phi\rho_g C_g]\frac{\partial T}{\partial t} = \frac{K_0}{\mathrm{RePr}}\lambda'\frac{\partial^2 T}{\partial x^2} - \phi\rho_g C_\mathrm{m}\left(u\frac{\partial T}{\partial x}\right), \tag{5}$$

where ρ_g and C_g are the density and heat capacity of the gas at constant pressure, ρ_m and C_m are the corresponding quantities in the solid matrix, ϕ is the porosity value and u is the gas axial filtration velocity. Additionally, $K_0 \simeq 1$ is a constant defined in [41], Re and Pr are the Reynolds and Prandtl numbers, $\lambda' = (1-\phi)\lambda_m + \phi\lambda_g$.

Therefore, the convective contributions could present a significant problem in the quantification of thermal diffusivity in porous materials. Another possibility is forced convection. Since, at low temperature, the heat losses under vacuum are near-zero, the Biot numbers calculated by solving the inverse problem in Equation (1) could be representative of convective heat transfer either by forced or natural convection. The impact of forced convection on the thermal diffusivity measurements results in generally lower values, see Figure 4. At the same time, the error margin is too high to draw a definitive conclusion on this part. Regardless, since the gas flow rate is adjustable, it can be decreased to minimise forced convection.

5. Conclusions

Measuring thermal properties in highly-porous solids with the flash method remains problematic. Even under vacuum, the complex microgeometry of porous materials manifests in the experimental temperature transients deviating from the expected model behaviour. This odd behaviour appears irrespective of whether external pores are open or blocked. When measurements are conducted under a gas environment, the gas infiltrates the open pores (if any are accessible) and participates in the transient heat transfer caused by the thermal flash. When a model accounting only for solid conduction is used to describe the transients, its intrinsic parameter and the "measurement" result, the thermal diffusivity a, stops being representative of just the solid material. Despite previous claims, the thermal diffusivity extracted from this model may not even be representative of the solid-gas mixture. This is caused by the non-linear terms in the coupled heat equation. An attempt was made to account for this nonlinearity using a simplified two-temperature model of coupled solid and gas conduction. Unfortunately, this model also produced solutions deviating from the experimental time-temperature profiles. This suggests two possibilities. Either convection should be accounted for during measurements of highly-porous solids — or the microgeometry of the pores needs to be explicitly accounted for in the heat equation. It is hoped that future work might address these possibilities.

Acknowledgements

We wish to acknowledge Exxentis AG for providing the alloy foam samples. We appreciate the help of Patrick Schütz and Uwe Beck from Netzsch-Gerätebau for preparing the samples used in this paper. We greatly appreciate discussions with Dr Vadim Zborovskii (Lebedev Physical Institute) who helped better understand the physical phenomenon under study.

References

[1] A. Lunev, A. Lauerer, V. Zborovskii, F. Léonard, Digital twin of a laser flash experiment helps to assess the thermal performance of metal foams, International Journal of Thermal Sciences 181 (2022) 107743. doi:https://doi.org/10.1016/j.ijthermalsci.2022.107743.
URL https://www.sciencedirect.com/science/article/pii/S1290072922002769

[2] A. Lunev, V. Mikhalchik, A. Tenishev, V. Baranov, Kinetic and microstructural studies of thermal decomposition in uranium mononitride compacts subjected to heating in high-purity helium, Journal of Nuclear Materials 475 (2016) 266–273. doi:10.1016/j.jnucmat.2016.04.018.
URL https://doi.org/10.1016/j.jnucmat.2016.04.018

[3] J. Marsh, R. Turner, J. Carter, M. Jenkins, Thermal diffusivity and secondary crystallisation kinetics in poly(lactic acid), Polymer 179 (2019) 121595. doi:10.1016/j.polymer.2019.121595.

[4] X. Wu, C. Wang, Y. Wang, Y. Zhu, Experimental study of thermo-physical properties and application of paraffin-carbon nanotubes composite phase change materials, International Journal of Heat and Mass Transfer 140 (2019) 671–677. doi:10.1016/j.ijheatmasstransfer.2019.06.008.

[5] R. K. Weese, A. K. Burnham, H. C. Turner, T. D. Tran, Exploring the physical, chemical and thermal characteristics of a new potentially insensitive high explosive RX-55-AE-5, Journal of Thermal Analysis and Calorimetry 89 (2) (2007) 465–473. doi:10.1007/s10973-006-8163-4.
URL https://doi.org/10.1007/s10973-006-8163-4

[6] P. Zbińkowski, J. Zmywaczyk, P. Koniorczyk, Experimental investigations of thermophysical properties of some paraffin waxes industrially manufactured in Poland, AIP Conference Proceedings 1866 (1) (2017) 040044. arXiv:https://aip.scitation.org/doi/pdf/10.1063/1.4994524, doi:10.1063/1.4994524.
URL https://aip.scitation.org/doi/abs/10.1063/1.4994524

[7] I. Kholmanov, J. Kim, E. Ou, R. S. Ruoff, L. Shi, Continuous carbon nanotube–ultrathin graphite hybrid foams for increased thermal conductivity and suppressed subcooling in composite phase change materials, ACS Nano 9 (12) (2015) 11699–11707. doi:10.1021/acsnano.5b02917.
URL https://doi.org/10.1021/acsnano.5b02917

[8] M. Drajewicz, K. Dychtoń, M. Góral, Thermal properties of YSZ powders for plasma spraying, Solid State Phenomena 227 (2015) 413–416. doi:10.4028/www.scientific.net/ssp.227.413.
URL https://doi.org/10.4028/www.scientific.net/ssp.227.413

[9] F. Cernuschi, P. Bison, A. Moscatelli, Microstructural characterization of porous thermal barrier coatings by laser flash technique, Acta Materialia 57 (12) (2009) 3460–3471. doi:10.1016/j.actamat.2009.03.041.
URL https://doi.org/10.1016/j.actamat.2009.03.041

[10] J. Mora-Monteros, C. Suter, S. Haussener, Effective conductivity of porous ceramics in a radiative environment, Ceramics International 46 (3) (2020) 2805–2815. doi:10.1016/j.ceramint.2019.09.272.

[11] M. Sans, V. Schick, G. Parent, O. Farges, Experimental characterization of the coupled conductive and radiative heat transfer in ceramic foams with a flash method at high temperature, International Journal of Heat and Mass Transfer 148 (2020) 119077. doi:10.1016/j.ijheatmasstransfer.2019.119077.

[12] R. Dyga, M. Płaczek, Heat transfer through metal foam–fluid system, Experimental Thermal and Fluid Science 65 (2015) 1–12. doi:10.1016/j.expthermflusci.2015.02.021.

[13] K. Wan, J. Chen, Z. Miao, Q. He, J. Tian, Experimental investigation of the effects of temperature, moisture, and physical structure variations on the thermal properties of lignite, Energy & Fuels 31 (7) (2017) 7052–7059. doi:10.1021/acs.energyfuels.7b01177.

[14] L. Wang, M. Gandorfer, T. Selvam, W. Schwieger, Determination of faujasite-type zeolite thermal conductivity from measurements on porous composites by laser flash method, Materials Letters 221 (2018) 322–325. doi:10.1016/j.matlet.2018.03.157.

[15] Q. Zhang, D. Yan, Temperature dependence of thermal diffusivity of OPC and CAC cement paste, Advances in Cement Research 28 (9) (2016) 576–582. doi:10.1680/jadcr.15.00146.

[16] J. E. Martínez-Martínez, F. P. Á. Rabanal, M. Lázaro, M. Alonso-Martínez, D. Alvear, J. J. del Coz-Díaz, Assessment of lightweight concrete thermal properties at elevated temperatures, Applied Sciences 11 (21) (2021) 10023. doi:10.3390/app112110023.

[17] T. A. Semelsberger, M. Veenstra, C. Dixon, Room temperature thermal conductivity measurements of neat MOF-5 compacts with high pressure hydrogen and helium, International Journal of Hydrogen Energy 41 (8) (2016) 4690–4702. doi:10.1016/j.ijhydene.2015.12.059.

[18] C. Zhao, T. Lu, H. Hodson, Natural convection in metal foams with open cells, International Journal of Heat and Mass Transfer 48 (12) (2005) 2452–2463. doi:10.1016/j.ijheatmasstransfer.2005.01.002.
URL https://doi.org/10.1016/j.ijheatmasstransfer.2005.01.002

[19] R. D. Cowan, Pulse method of measuring thermal diffusivity at high temperatures, Journal of Applied Physics 34 (4) (1963) 926–927. doi:10.1063/1.1729564.
URL https://doi.org/10.1063/1.1729564

[20] J. A. Cape, G. W. Lehman, Temperature and finite pulse-time effects in the flash method for measuring thermal diffusivity, Journal of Applied Physics 34 (7) (1963) 1909–1913. doi:10.1063/1.1729711.
URL https://doi.org/10.1063/1.1729711

[21] V. Mityushev, N. Rylko, Maxwell's approach to effective conductivity and its limitations, The Quarterly Journal of Mechanics and Applied Mathematics 66 (2) (2013) 241–251. doi:10.1093/qjmam/hbt003.
URL https://doi.org/10.1093/qjmam/hbt003

[22] V. Mityushev, Effective properties of two-dimensional dispersed composites. part II. revision of self-consistent methods, Computers &amp Mathematics with Applications 121 (2022) 74–84. doi:10.1016/j.camwa.2022.07.003.
URL https://doi.org/10.1016/j.camwa.2022.07.003

[23] R. Kovács, A. Fehér, S. Sobolev, On the two-temperature description of heterogeneous materials, International Journal of Heat and Mass Transfer 194 (2022) 123021. doi:https://doi.org/10.1016/j.ijheatmasstransfer.2022.123021.
URL https://www.sciencedirect.com/science/article/pii/S001793102200494X

[24] A. Fehér, N. Lukács, L. Somlai, T. Fodor, M. Szücs, T. Fülöp, P. Ván, R. Kovács, Size effects and beyond-fourier heat conduction in room-temperature experiments, Journal of Non-Equilibrium Thermodynamics 46 (4) (2021) 403–411. doi:10.1515/jnet-2021-0033.
URL https://doi.org/10.1515/jnet-2021-0033

[25] S. Both, B. Czél, T. Fülöp, G. Gróf, Á. Gyenis, R. Kovács, P. Ván, J. Verhás, Deviation from the fourier law in room-temperature heat pulse experiments, Journal of Non-Equilibrium Thermodynamics 41 (1). doi:10.1515/jnet-2015-0035.
URL https://doi.org/10.1515/jnet-2015-0035

[26] S. Min, J. Blumm, A. Lindemann, A new laser flash system for measurement of the thermophysical properties, Thermochimica Acta 455 (1-2) (2007) 46–49. doi:10.1016/j.tca.2006.11.026.

[27] J. Blumm, D. Morgan, Thermal conductivity measurement techniques, in: Thermal Conductivity 27: Thermal Expansion 15: Joint Confer-

ences, October 26-29, 2003, Knoxville, Tennessee, USA, DEStech Publications, Inc, 2005, p. 83.

[28] H. Wang, W. D. Porter, R. B. Dinwiddie, Laser-induced pressure-wave and barocaloric effect during flash diffusivity measurements, Applied Physics Letters 111 (5) (2017) 051901. doi:10.1063/1.4991352.

[29] A. Lunev, V. Zborovskii, T. Aliev, R. Heymer, O. Vilkhivskaya, PULsE: An open-source software for laser flash analysis, Software Impacts 6 (2020) 100044. doi:10.1016/j.simpa.2020.100044.

[30] A. Lunev, kotik-coder/pulse: Pulse v1.93f : fixes (Dec. 2021). doi:10.5281/zenodo.5784553.
URL https://doi.org/10.5281/zenodo.5784553

[31] A. Salazar, A. Mendioroz, E. Apiñaniz, C. Pradere, F. Noël, J.-C. Batsale, Extending the flash method to measure the thermal diffusivity of semitransparent solids, Measurement Science and Technology 25 (3) (2014) 035604. doi:10.1088/0957-0233/25/3/035604.

[32] R. L. McMasters, J. V. Beck, R. B. Dinwiddie, H. Wang, Accounting for penetration of laser heating in flash thermal diffusivity experiments, Journal of Heat Transfer 121 (1) (1999) 15–21. doi:10.1115/1.2825929.

[33] A. Lunev, R. Heymer, Decreasing the uncertainty of classical laser flash analysis using numerical algorithms robust to noise and systematic errors, Review of Scientific Instruments 91 (6) (2020) 064902. doi:10.1063/1.5132786.

[34] B. Liao, J. Zhou, G. Chen, Generalized two-temperature model for coupled phonon-magnon diffusion, Physical Review Letters 113 (2). doi:10.1103/physrevlett.113.025902.
URL https://doi.org/10.1103/physrevlett.113.025902

[35] D. A. S. Rees, MICROSCOPIC MODELING OF THE TWO-TEMPERATURE MODEL FOR CONDUCTION IN HETEROGENEOUS MEDIA, Journal of Porous Media 13 (2) (2010) 125–143. doi:10.1615/jpormedia.v13.i2.40.
URL https://doi.org/10.1615/jpormedia.v13.i2.40

[36] N. Afrin, Y. Zhang, J. Chen, Dual-phase lag behavior of a gas-saturated porous-medium heated by a short-pulsed laser, International Journal of Thermal Sciences 75 (2014) 21–27. doi:10.1016/j.ijthermalsci.2013.07.019.
URL https://doi.org/10.1016/j.ijthermalsci.2013.07.019

[37] S. A. Rukolaine, Unphysical effects of the dual-phase-lag model of heat conduction, International Journal of Heat and Mass Transfer 78 (2014) 58–63. doi:10.1016/j.ijheatmasstransfer.2014.06.066.
URL https://doi.org/10.1016/j.ijheatmasstransfer.2014.06.066

[38] D. D. Joseph, L. Preziosi, Heat waves, Reviews of Modern Physics 61 (1) (1989) 41–73. doi:10.1103/revmodphys.61.41.
URL https://doi.org/10.1103/revmodphys.61.41

[39] W. J. Parker, R. J. Jenkins, C. P. Butler, G. L. Abbott, Flash method of determining thermal diffusivity, heat capacity, and thermal conductivity, Journal of Applied Physics 32 (9) (1961) 1679–1684. doi:10.1063/1.1728417.

[40] V. G. Baranov, Y. N. Devyatko, A. V. Tenishev, A. V. Khlunov, O. V. Khomyakov, New method for determining the temperature dependence of the thermal conductivity coefficient of dielectrics in a pulse experiment, Inorganic Materials: Applied Research 1 (2) (2010) 167–173. doi:10.1134/s2075113310020164.
URL https://doi.org/10.1134/s2075113310020164

[41] E. B. Soboleva, Rayleigh-darcy convection in a porous layer: A comparison of near-critical and normal fluid phases (2010). doi:10.48550/ARXIV.1001.4139.
URL https://arxiv.org/abs/1001.4139